Measurement of electron temperatures and electron energy distribution functions in dual frequency capacitively coupled CF_4/O_2 plasmas using trace rare gases optical emission spectroscopy

Zhiying Chen, Vincent M. Donnelly,[a)] and Demetre J. Economou[b)]
Department of Chemical and Biomolecular Engineering, Plasma Processing Laboratory, University of Houston, Houston, Texas 77204-4004

Lee Chen, Merritt Funk, and Radha Sundararajan
Tokyo Electron America, Austin, Texas 78741

(Received 28 April 2009; accepted 22 June 2009; published 31 July 2009)

Measurements of electron temperatures (T_e) and electron energy distribution functions (EEDFs) in a dual frequency capacitively coupled etcher were performed by using trace rare gas optical emission spectroscopy (TRG-OES). The parallel plate etcher was powered by a high frequency (60 MHz) "source" top electrode and a low frequency (13.56 MHz) "substrate" bottom electrode. T_e first increased with pressure up to $\sim$20 mTorr and then decreased at higher pressures. Increasing the bottom rf power resulted in higher electron temperatures. Electron temperatures in 90% CF_4 +10% O_2 plasmas were similar to those in 80% CF_4+20% O_2 plasmas. EEDF exhibited bi-Maxwellian characteristics with enhanced high energy tail, especially at pressures >20 mTorr. © *2009 American Vacuum Society.* [DOI: 10.1116/1.3179162]

I. INTRODUCTION

Dual frequency capacitively coupled plasmas (2f-CCPs) are commonly employed in the fabrication of modern integrated circuits.[1–5] These systems are attractive because quasi-independent control of ion flux and ion bombardment energy to the substrate can be realized. In 2f-CCP, the ion energy is controlled by the low frequency (LF) source, while the plasma density and ion flux are determined mainly by the high frequency (HF) source.

Many theoretical investigations of 2f-CCP have been carried out. Kawamura *et al.*[6] and Turner and Chabert[7,8] discussed electron heating mechanisms. Kawamura *et al.*[6] developed an analytical stochastic heating model that was in agreement with their particle-in-cell (PIC) simulation. Turner and Chabert[7] predicted that electron heating was enhanced by the two frequencies acting together. Turner and Chabert[8] also found that both collisionless and Ohmic heating increased with increasing low frequency power. Using a self-consistent PIC Monte Carlo collision (PIC-MCC) method, Wakayama and Nanbu[9] examined the dynamics of dual frequency (2/60 MHz) capacitively coupled plasmas in Ar (25 mTorr) by one- and two-dimensional simulations. The one-dimensional simulation showed that the electron density and plasma potential were modulated at both the low and high frequencies. The sheath became thicker as the LF amplitude was increased, but the peak ion density between the electrodes did not change significantly. The two-dimensional simulation revealed that the maximum energy of ions incident on the HF electrode was about 200 eV, whereas the energy of the ions incident on the LF electrode was widely distributed up to 850 eV. Lee *et al.*[10] investigated ion energy distributions, plasma densities, plasma potentials, and electron energy distribution functions (EEDFs) in 2f-CCP using a PIC-MCC simulation. The nonmonotonic behavior of plasma density versus LF voltage was attributed to the widening of the sheath, causing an increase in the power absorbed by ions accelerated in the sheath. Mussenbrock *et al.*[11] developed a nonlinear global (zero-dimensional) model of a 2f-CCP driven by the superposition of two sinusoidal radio-frequency (rf) voltages. They found that the power deposition into the discharge was nearly constant over the whole pressure range. In addition, an electron resonance due to the excitation of higher harmonics by the nonlinear interaction of bulk plasma and sheath was an efficient electron heating mechanism. Wu *et al.*[12] computed ion energy distributions in a 2f-CCP reactor based on a linear transfer function that related the time-varying sheath voltage to the time-varying ion energy at the surface.

On the other hand, there are very few experimental studies of 2f-CCP reported in the literature. Gans *et al.*[5] studied the frequency coupling in a short gap 2f-CCP etcher. A strong coupling of the two frequencies was observed in the plasma emission profiles. Consequently, the ionization dynamics and plasma density were determined by both frequencies. Hebner *et al.*[4] investigated a 2f-CCP (60/13 MHz) 300 mm wafer processing chamber. They reported the frequency dependence of line-integrated electron density, ion saturation current, optical emission, and argon metastable density. The electron density increased linearly with applied HF power between 20 and 200 mTorr. A linear increase in electron density with pressure for a constant HF power of 300 W was also observed. As the 13 MHz bias power was increased from 0 to 1500 W, the electron density was independent of bias power for fixed 60 MHz source power, except for the case of zero source power.

[a)]Electronic mail: vmdonnelly@uh.edu
[b)]Electronic mail: economou@uh.edu

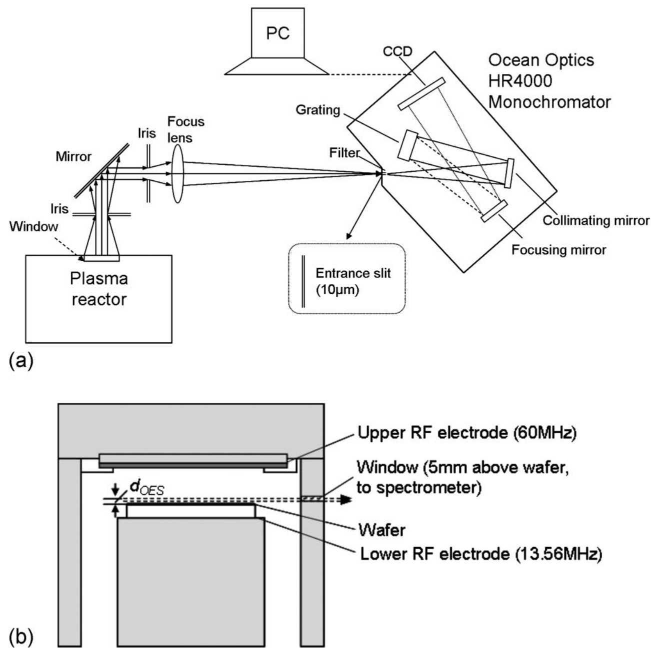

FIG. 1. (a) Schematic diagram of the overall experimental setup. (b) Schematic diagram of the plasma chamber. Dashed lines show the region above the substrate electrode from which optical emission was collected.

The electron temperature (T_e), or more generally the EEDF, determines the ionization, dissociation and excitation rates in a plasma, as well as the energy and flux of ions to the substrate. Therefore, accurate determination of T_e and the EEDF is important for understanding plasma behavior and optimizing plasma processes. In this work, measurements of T_e in CF_4/O_2 plasmas generated in a 2f-CCP etcher are reported as a function of pressure, applied rf power, and O_2 feed gas content. Trace rare gases optical emission spectroscopy (TRG-OES) was used to determine electron temperatures and derive approximate EEDF. Unlike the traditional Langmuir probe technique, TRG-OES is a nonintrusive method,[13,14] based on a comparison of atomic emission intensities (from trace amounts of rare gases added to the plasma) with intensities calculated from a model.

II. EXPERIMENT

A schematic diagram of the experimental setup is shown in Fig. 1. The 2f-CCP parallel plate etcher had a top showerhead electrode powered at 60 MHz (source power) and a bottom substrate electrode powered at 13.56 MHz (bias power). In most experiments, the interelectrode gap l was 80 mm. In a few cases the gap was extended to values between $l=80$ and 195 mm. 80% CF_4+20% O_2 or 90% CF_4 +10% O_2 (by volume) plasmas were ignited at pressures ranging from 4 to 200 mTorr, two different top rf powers (500 and 1000 W), and four different bottom rf powers (0, 100, 300, and 500 W). In all experiments, the total (CF_4 +O_2) flow rate was 95 SCCM (SCCM denotes cubic centimeter per minute at STP).

Optical emission from CF_4/O_2 plasmas was recorded by an Ocean Optics HR4000 spectrometer. The spectrometer had a spectral response in the 7350–9150 Å range. The spectral resolution was 1.6 Å with a 10 μm entrance slit. The detector was a Toshiba TCD1304AP linear charge coupled device array (3648 pixels, pixel size: 8×200 μm^2). Plasma induced emission was reflected by a mirror and focused onto the entrance slit of the spectrometer. Emission intensities were corrected for the relative response of the spectrometer and detector. Line-integrated emission was collected at a distance of $d_{OES}=l-75$mm above the bottom electrode as shown in Fig. 1(b). In most of the measurements presented here, $l=80$ mm; consequently $d_{OES}=5$ mm.

TRG-OES measurements were performed by adding a small amount (5% by volume, i.e., 5 SCCM) of a mixture containing 40% Ne, 20% Ar, 20% Kr, and 20% Xe (by volume) to the CF_4/O_2 feed gas. Details of electron temperature measurements by TRG-OES have been reported previously.[13,14] Briefly, optical emission intensities from the Paschen $2p_x$ ($x=1-10$) levels of Ar, Kr, and Xe were computed from a model, assuming a Maxwellian electron energy distribution, and then compared to the measured intensities. T_e in the model was adjusted until the best match was obtained between the computed and observed relative emission intensities. Previous measurements in oxygen plasmas demonstrated that addition of the rare gas mixture did not significantly perturb the properties of the pure discharge.[15]

III. RESULTS AND DISCUSSION

A. Emission spectra

Figure 2(a) shows an optical emission spectrum from a 100 mTorr 80% CF_4+20% O_2 plasma with 1000 W top rf power and 500 W bottom rf power. Atomic fluorine (7399, 7426, 7552, 7573, 775, and 7800 Å) and atomic oxygen (7772 and 8446 Å) emission lines are clearly observed. Other lines are from the TRG mixture. Figure 2(b) is a portion of Fig. 2(a) that includes several of the rare gas emission lines: Ar (8115 Å), Kr (8104, 8113, and 8190 Å), and Xe (8231 Å). The intensities of these and other rare gas lines were used to determine the electron temperature, as listed in Table I, and discussed below.

B. Electron temperature

In most of the prior application of the TRG-OES method for electron temperature measurements, the plasmas were inductively coupled.[13–15] At some distance from the inductive coil, these plasmas tend to have an EEDF that is either Maxwellian or has suppressed high energy electron population relative to a Maxwellian. On the other hand, capacitively coupled plasmas at sufficiently low pressures and high rf voltages, as in the present study, can have EEDF that deviates substantially from a Maxwellian. For example, the population of high energy electrons can increase due to stochastic heating resulting from the expanding and contracting sheaths. This effect can be enhanced in dual frequency plasmas.[7,8] In addition, secondary electrons created by ion bombardment of the momentary cathode can accelerate to the full sheath potential (several hundred eV at the peak of

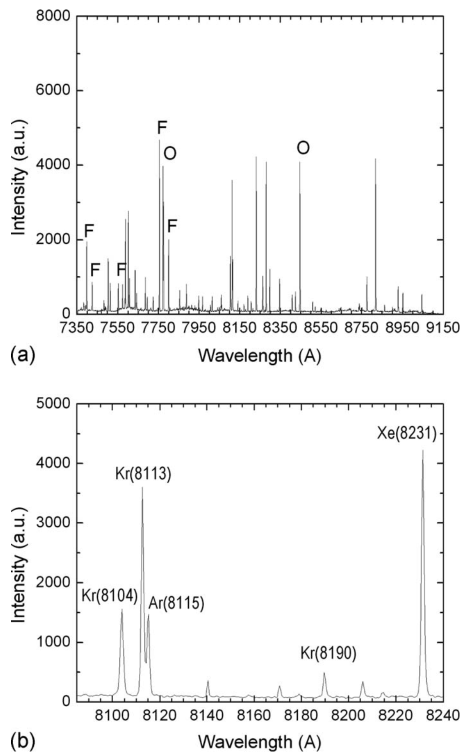

FIG. 2. (a) Optical emission spectrum from a 100 mTorr 80% CF_4 +20% O_2 plasma with 1000 W top rf power and 500 W bottom rf power. (b) A portion of the spectrum in (a) that includes several rare gas emission lines.

the applied rf voltage) and enter the plasma, creating a (usually small) population of very high energy electrons. Langmuir probes cannot detect these electrons, since they will be masked by a large positive ion current. Electrons with these

TABLE I. Emitting levels and lines used to determine electron temperatures. The lines used to determine T_e and T_e^{high} (lines excited primarily from ground states) are shown by check (✓) marks.

Gas	State	λ_1 (Å)	λ_2 (Å)	T_e	T_e^{high}
Ar	$2p_1$	7504			✓
	$2p_5$	7515			✓
	$2p_9$	8115		✓	
	$2p_8$	8424	8014	✓	
	$2p_4$	8521	7948	✓	
Kr	$2p_5$	7587			✓
	$2p_6$	7601	8190		
	$2p_1$	7685			✓
	$2p_7$	7694	8298		✓
	$2p_3$	7854		✓	
	$2p_9$	8113		✓	
	$2p_4$	8509		✓	
Xe	$2p_6$	8232		✓	
	$2p_5$	8280			✓
	$2p_3$	8347			✓
	$2p_8$	8819		✓	
	$2p_9$	9045		✓	

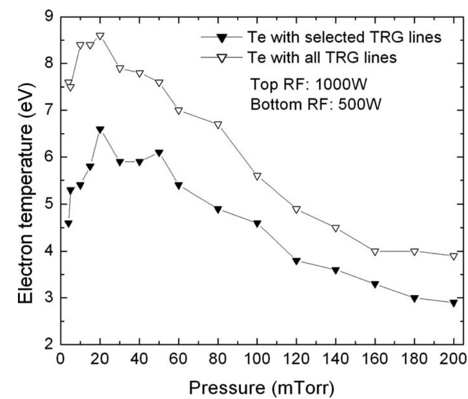

FIG. 3. Electron temperature as a function of pressure in an 80% CF_4 +20% O_2 plasma with 1000 W top rf power and 500 W bottom rf power. Values of electron temperature derived from all observable rare gas lines are compared with those (hereafter designated as T_e) obtained with selected emission lines that minimize contributions from high energy electrons ($>\sim 40$ eV).

high energies do excite optical emission, however, and so are folded into an electron "temperature" by a nonselective application of the TRG-OES method.

To minimize this complication, the set of 90 cross sections for electron impact excitation of the 10 Paschen $2p$ levels for Ar, Kr, and Xe from the ground state, the $^3P_0$ metastable state, and the $^3P_2$ metastable state was screened for those cross sections that are least sensitive to high energy electrons ($>\sim 40$ eV) relative to low energy electrons. This set of emission lines is denoted as T_e in Table I. T_e derived from these lines represents an "average" electron temperature over the bulk of the EEDF with minimum contributions from any high energy secondaries.

Figure 3 illustrates this effect. Electron temperatures in 80% CF_4+20% O_2 plasmas (1000 W top power and 500 bottom power) using all TRG emission lines are compared with those obtained using selected emission lines (T_e in Table I) with cross sections that are less sensitive to high energy electrons. Throughout the range of pressure, T_e values derived using all emission lines are higher than T_e determined with the selected emission line set, presumably due at least in part to the contributions from high energy secondaries.

Since the discharge close to the substrate is the main focus in this study, most OES measurements were made along a line at a short distance (d_{OES}=5 mm) from the substrate. At the same time, it is important that the observation region does not include the plasma sheath, as this is a region of dramatically reduced electron density and increased electron energies, complicating the application of the TRG-OES method. To verify that the light collection region did not overlap with the sheath, some measurements were made as a function of distance from the bottom electrode (d_{OES} =5–120 mm). This was accomplished by moving the bottom electrode, thereby increasing the interelectrode gap from 80 to 195 mm. T_e measurements as a function of gap are presented in Fig. 4, along with relative Ar 7504 Å emission intensities (I_{Ar}). There are no spikes in T_e nor precipitous

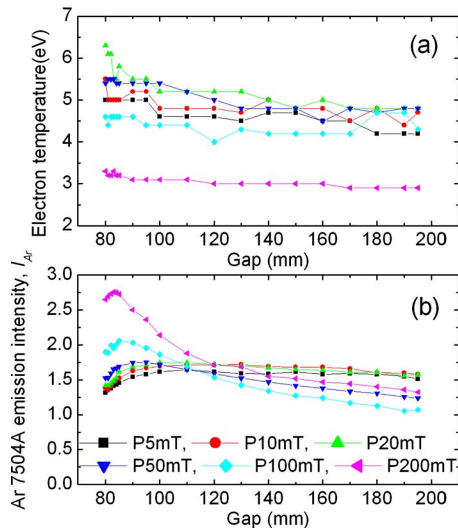

FIG. 4. (Color online) (a) Electron temperature and (b) Ar 7504 Å emission intensity as a function of interelectrode gap in an 80% CF_4+20% O_2 plasma with 500/500 W top/bottom rf powers and varying pressure.

drops in I_{Ar} that would indicate a significant encroachment into the sheath region at the smallest gap; hence all remaining measurements were done at a gap of 80 mm, corresponding to $d_{OES}=5$ mm. A small, gradual falloff in T_e is evident in Fig. 4, as the characteristic length for electron diffusion increases at larger gaps. Similarly, the falloff in I_{Ar} near the electrode is small. At low pressures, I_{Ar} is nearly independent of gap, while at high pressures it falls off away from the electrode, most likely due to the small falloff in T_e (note that I_{Ar} is more sensitive to T_e at low T_e).

T_e values in 80% CF_4+20% O_2 plasmas were measured as a function of pressure and bottom (13.56 MHz) rf power at top (60 MHz) rf powers of 1000 W (Fig. 5) and 500 W (Fig. 6). Above 20 mTorr, T_e varies inversely with pressure, while below 20 mTorr, T_e decreases somewhat with decreasing pressure, especially with 500 W applied to the top electrode and at least 100 W power applied to the bottom electrode. Comparable sets of T_e measurements for 90% CF_4 +10% O_2 plasmas are presented in Figs. 7 and 8, with 1000

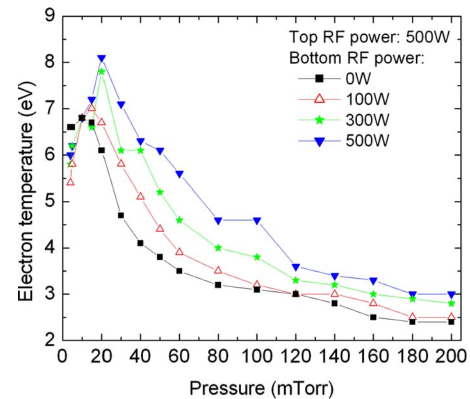

FIG. 6. (Color online) Electron temperature as a function of pressure in an 80% CF_4+20% O_2 plasma with 500 W top rf power and varying (0–500 W) bottom rf power.

and 500 W top rf powers, respectively. The T_e values and trends are very similar to the 80% CF_4+20% O_2 plasma shown in Figs. 5 and 6. Below ~70 mTorr, T_e in 90% CF_4+10% O_2 plasmas are ~2%–10% higher than for 80% CF_4+20% O_2 plasmas.

There are surprisingly few reports of electron temperatures (or EEDF) in CF_4 CCP and none to our knowledge in CF_4/O_2 CCP. The T_e values measured in the present study and reported by others are high relative to those in Ar CCP or generally in inductively coupled plasma reactors.[16–18] Descoeudres *et al.*[19] computed T_e values of 6 eV at 76 mTorr and 4.8 eV at 200 mTorr in a 13.56 MHz (single frequency) discharge with a gap of 4 cm. So *et al.*[20,21] modeled a 200 mTorr, 13.56 MHz CF_4 CCP with a 2 cm gap and computed a T_e of 6 eV in the bulk plasma. The lower T_e values measured in the present study with power applied just to the upper electrode (single frequency discharge) could be due to the larger gap (8 vs 2 cm) or the higher frequency (60 vs 13.56 MHz) used in the present work.

Above 20 mTorr, T_e varies inversely with pressure (Figs. 5–8), as required under the simplest of circumstances, when the need to balance electron generation and loss requires a smaller ionization rate constant (and hence a lower T_e), to

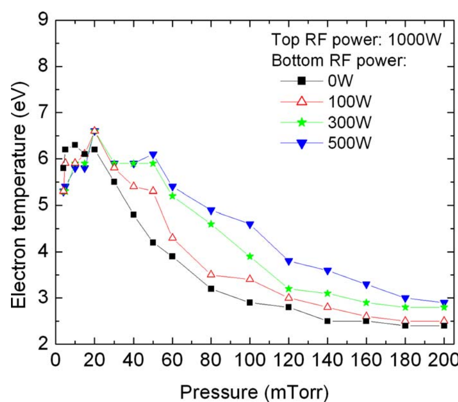

FIG. 5. (Color online) Electron temperature as a function of pressure in an 80% CF_4+20% O_2 plasma with 1000 W top rf power and varying (0–500 W) bottom rf power.

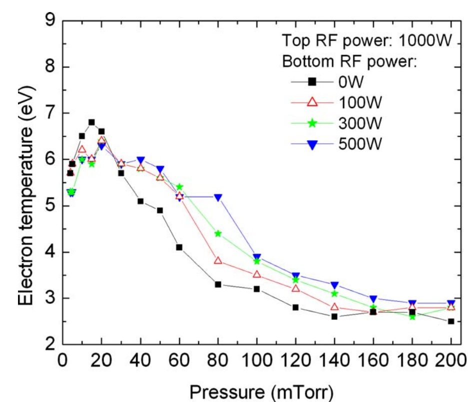

FIG. 7. (Color online) Electron temperature as a function of pressure in a 90% CF_4+10% O_2 plasma with 1000 W top rf power and varying (0–500 W) bottom rf power.

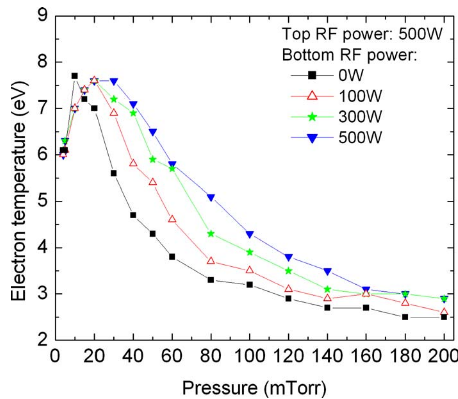

FIG. 8. (Color online) Electron temperature as a function of pressure in a 90% CF_4+10% O_2 plasma with 500 W top rf power and varying (0–500 W) bottom rf power.

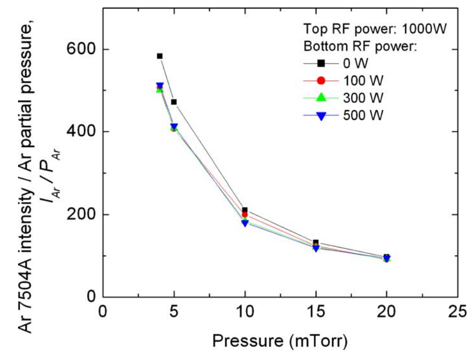

FIG. 9. (Color online) Ratio of the relative Ar 7504 Å emission intensity to Ar partial pressure in an 80% CF_4+20% O_2 plasma with 1000 W top rf power and varying (0–500 W) bottom rf power.

compensate for the higher gas number density at higher pressure. Below 20 mTorr, Figs. 5–8 (particularly Figs. 6 and 8 at lower top power) show that T_e generally decreases with decreasing pressure. This could be due to the electronegative nature of the CF_4/O_2 plasma. The structure of an electronegative discharge is stratified,[22] consisting of a central electronegative core and an electropositive edge. This structure, however, can change as pressure and/or power vary. Denpoh and Nanbu[23] found through simulations that when the pressure decreased to 50 mTorr, a CF_4 CCP discharge changed from electronegative to electropositive. This transition was accompanied by a drastic increase in electron density (in excess of the negative ion density), a disappearance of the stratified structure, a lower bulk electric field, and a reduction in electron temperature, ascribed to much lower Joule heating in the bulk. Calculation by Franklin[24] illustrated that larger electronegativity corresponds to a higher T_e. Picard *et al.*[25] found that T_e rose from ~3 to 9 eV as plasma electronegativity increased by going from an Ar CCP to a pure SF_6 CCP, accompanied by a 200-fold reduction in electron density at nearly constant positive ion density. Jauberteau *et al.* measured the ratio of negative ion density to electron density in a CF_4 CCP and found that it increased with increasing pressure below 30 mTorr.[26] Based on these results, the behavior of T_e with pressure below 20 mTorr in the present study may be due to changes in the plasma electronegativity. As pressure increases and top rf power decreases, the plasma becomes progressively more electronegative, resulting in higher electron temperatures.

At pressures below 20 mTorr, the bottom power seems to have relatively little effect on T_e. Under these conditions, for levels that are mainly populated by electron impact excitation from the ground state (e.g., Ar $2p_1$ at 7504 Å), the relative optical emission intensity divided by the rare gas partial pressure is a measure of relative electron density. Measurements of I_{Ar}/P_{Ar} (where P_{Ar} is the Ar partial pressure) are presented in Fig. 9. At a given pressure, the values are nearly independent of bottom power, indicating that this power has little effect on the electron density. The strong decrease in I_{Ar}/P_{Ar} with increasing pressure is also an indication that the plasma becomes increasingly electronegative.

At pressures above 20 mTorr, for a given top power of 500 or 1000 W, higher bottom electrode (low frequency) rf power results in higher T_e (Figs. 5–8). This behavior may be explained by enhanced heating of electrons by the spatially oscillating sheath, with increasing low frequency voltage. Lee *et al.*[10] simulated capacitively coupled single- and dual frequency (27/2 MHz) rf discharges and found that increasing the low frequency voltage also led to an increase in T_e. Using a one-dimensional PIC-MCC simulation, Kim *et al.*[27] similarly reported an increasing T_e with low frequency voltage in a 2f-CCP (27/2 MHz). Their results showed that the sheath width increased by increasing the low frequency voltage, accompanied by a decrease in plasma density. A thicker sheath enhances stochastic heating of electrons leading to higher electron temperature. The enhanced heating by the bottom electrode (low frequency) rf power at high pressures compared with little or no heating at low pressures can be explained by a reduction in electron density due to increased attachment at high pressure. This causes the sheath width to increase, which leads to an increase in the velocity of the periodic sheath expansion, which in turn causes enhanced stochastic electron heating.

C. Electron energy distribution

The electron temperatures reported above were calculated by TRG-OES based on the rare gas emission lines shown in Table I under T_e, assuming a Maxwellian EEDF. However, notwithstanding the small population of very high energy secondary electrons, the EEDF in CCP reactors is frequently not Maxwellian. For example, a bi-Maxwellian distribution in Ar plasmas was observed as the gas pressure varied in the range of 70–400 mTorr, while a Druyvesteyn distribution was found above 500 mTorr.[16] CF_4 2f-CCP (100/1 MHz) PIC simulations showed a bi-Maxwellian distribution at with 0–800 V on the LF electrode and 100 V on the HF electrode.[28] A simulation of 2f-CCP in Ar revealed that as the LF (2 MHz) current increased for a fixed HF (27 MHz) current, the EEDF changed from Druyvesteyn to bi-Maxwellian (in the absence of secondary electron emission) or Maxwell-

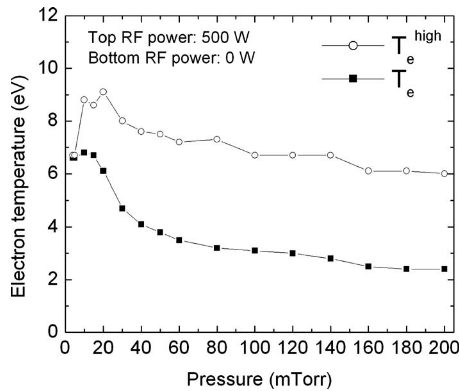

FIG. 10. Electron temperatures as a function of pressure in an 80% CF_4 +20% O_2 plasma with 500 W top rf power and no bottom rf power. Squares: T_e, determined from the set of emission lines checked in Table I; circles: T_e^{high}, determined from rare gas emission lines excited mostly from the ground states (also checked in Table I).

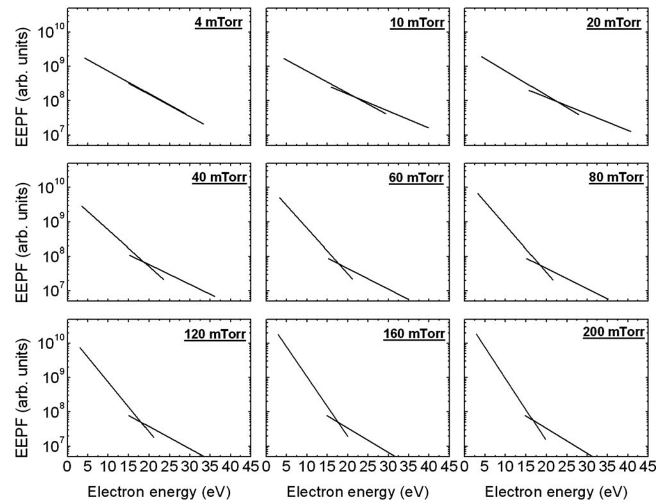

FIG. 12. Approximate EEDF as a function of pressure in an 80% CF_4 +20% O_2 plasma with 500 W top rf power and no bottom rf power. The EEDFs were constructed using the T_e^{high} and T_e values of Fig. 10.

ian type (in the presence of secondary electron emission), along with a significant drop in the effective electron temperature.[29] Under conditions such as described above, a single T_e is not adequate to describe the electron population.

A low-resolution EEDF can be obtained through further consideration of the contribution from higher energy electrons. An electron temperature T_e^{high} was determined by using the emission lines excited mostly from ground states,[30] namely, $2p_1$ for Ar (7504 Å) and Kr (7685 Å), $2p_5$ for Ar (7515 Å), Kr (7587 Å), and Xe (8280 Å), $2p_7$ for Kr (7694 and 8298 Å), and $2p_3$ for Xe (8347 Å) (see Table I). T_e^{high} represents electron energies in the high energy portion of the EEDF, ~15–40 eV. T_e^{high} and T_e were combined to obtain approximate EEDF for CF_4/O_2 plasmas in 2f-CCP.

Figure 10 shows T_e^{high} and T_e as a function of pressure for a 80% CF_4+20% O_2 plasma with 500 W top rf power and no bottom rf power. Below ~20 mTorr, T_e^{high} is close to T_e. Above 20 mTorr, T_e^{high} is considerably higher than T_e, which implies a high energy tail in the EEDF. Figure 11 shows T_e^{high} and T_e as a function of pressure for a 80% CF_4+20% O_2 plasma with 500 W top rf power and 300 W bottom rf power. T_e^{high} is higher than that in CF_4/O_2 plasma with no bottom rf power (compare to Fig. 10). This indicates that there are more electrons in the high energy tail with 300 W bottom rf power compared to no bottom power. In low pressure capacitive discharges, stochastic heating is enhanced by dual frequency excitation.[6,7] The high frequency motion generates stochastic heating while the low frequency motion enhances that heating by widening the sheath and transporting oscillating electrons to regions of lower plasma density, hence higher sheath velocity. This could explain the higher values of T_e^{high} when rf power is applied to the bottom electrode.

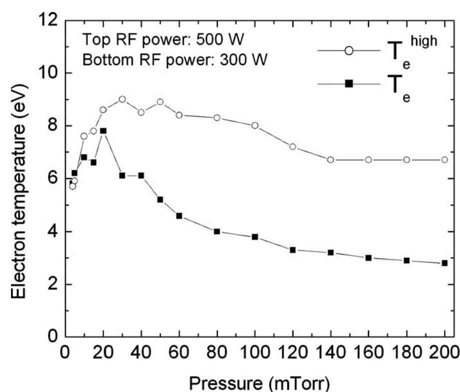

FIG. 11. Electron temperatures as a function of pressure in an 80% CF_4 +20% O_2 plasma with 500 W top rf power and 300 W bottom rf power. Squares: T_e, determined from the set of emission lines checked in Table I; circles: T_e^{high}, determined from rare gas emission lines excited mostly from the ground states (also checked in Table I).

The T_e^{high} and T_e values of Fig. 10 were then used to construct approximate EEDF. Figure 12 shows such EEDF for a 80% CF_4+20% O_2 plasma, with 500 W top rf power and no bottom power, as a function of pressure. The slopes of the two lines are equal to $-1/T_e^{high}$ and $-1/T_e$ in the high and low energy ranges, respectively. The end points of the lines correspond to the energy ranges for T_e^{high} (~15–40 eV) and T_e (~3–28 eV). Electrons within these ranges are responsible for 80% of the computed emission. These ranges were estimated from a procedure that was described previously.[30]

Below ~20 mTorr the EEDF is approximately Maxwellian with a slightly enhanced tail. Above 20 mTorr, the EEDF exhibits a clear bi-Maxwellian character with enhanced high energy tail, which could be caused by the change in discharge characteristics and stochastic heating, as discussed above. Such bi-Maxwellian EEDF were predicted by a PIC-MCC simulation of a 2f-CCP CF_4 discharge for pressures of 30 and 50 mTorr.[28]

IV. SUMMARY AND CONCLUSIONS

The electron temperature in dual frequency (60/13.56 MHz) capacitively coupled CF_4/O_2 plasmas was determined as a function of pressure (4–200 mTorr) at different applied top (500 and 1000 W) and bottom (0–500 W) rf powers and

two oxygen contents (10% and 20% by volume) by using TRG-OES. Below 20 mTorr, the electron temperature T_e increased with increasing pressure. The dependence of plasma electronegativity on pressure may be responsible for this behavior. T_e decreased rapidly with increasing pressure in the 20–60 mTorr range and then slowly decreased with further increases in pressure to 200 mTorr. Increasing the applied bottom rf power resulted in higher electron temperature. Over the whole pressure range investigated, the T_e in 90% CF_4+10% O_2 plasmas was very similar to that in 80% CF_4+20% O_2 plasmas.

Approximate EEDF for 80% CF_4+20% O_2 plasmas as a function of pressure were also constructed. The high energy tail of the EEDF was obtained by selecting rare gas emission lines originating mostly from ground states. The EEDF exhibited a bi-Maxwellian character with a enhanced high energy tail, especially above 20 mTorr.

ACKNOWLEDGMENTS

Financial support of this work by Tokyo Electron America is gratefully acknowledged.

[1]H. H. Goto, H.-D. Lowe, and T. Ohmi, J. Vac. Sci. Technol. A **10**, 3048 (1992).
[2]W. Tsai, G. Mueller, R. Lindquist, and B. Frazier, J. Vac. Sci. Technol. B **14**, 3276 (1996).
[3]K. Maeshige, G. Washio, T. Yagisawa, and T. Makabe, J. Appl. Phys. **91**, 9494 (2002).
[4]G. A. Hebner, E. V. Barnat, P. A. Miller, A. M. Paterson, and J. P. Holland, Plasma Sources Sci. Technol. **15**, 879 (2006).
[5]T. Gans, J. Schulze, D. O'Connell, U. Czarnetzki, R. Faulkner, A. R. Ellingboe, and M. M. Turner, Appl. Phys. Lett. **89**, 261502 (2006).
[6]E. Kawamura, M. A. Lieberman, and A. J. Lichtenberg, Phys. Plasmas **13**, 053506 (2006).
[7]M. M. Turner and P. Chabert, Phys. Rev. Lett. **96**, 205001 (2006).
[8]M. M. Turner and P. Chabert, Appl. Phys. Lett. **89**, 231502 (2006).
[9]G. Wakayama and K. Nanbu, IEEE Trans. Plasma Sci. **31**, 638 (2003).
[10]J. K. Lee, N. Y. Babaeva, H. C. Kim, O. V. Manuilenko, and J. W. Shon, IEEE Trans. Plasma Sci. **32**, 47 (2004).
[11]T. Mussenbrock, D. Ziegler, and R. P. Brinkmann, Phys. Plasmas **13**, 083501 (2006).
[12]A. C. F. Wu, M. A. Lieberman, and J. P. Verboncoeur, J. Appl. Phys. **101**, 056105 (2007).
[13]M. V. Malyshev and V. M. Donnelly, J. Vac. Sci. Technol. A **15**, 550 (1997).
[14]M. V. Malyshev and V. M. Donnelly, Phys. Rev. E **60**, 6016 (1999).
[15]N. C. M. Fuller, M. V. Malyshev, V. M. Donnelly, and I. P. Herman, Plasma Sources Sci. Technol. **9**, 116 (2000).
[16]V. A. Godyak and R. B. Piejak, Phys. Rev. Lett. **65**, 996 (1990).
[17]T. Kimura and M. Noto, J. Appl. Phys. **100**, 063303 (2006).
[18]T. Kimura and K. Ohe, J. Appl. Phys. **92**, 1780 (2002).
[19]A. Descoeudres, L. Sansonnens, and Ch. Hollenstein, Plasma Sources Sci. Technol. **12**, 152 (2003).
[20]S.-Y. So, A. Oda, H. Sugawara, and Y. Sakai, J. Phys. D **35**, 2978 (2002).
[21]S.-Y. So, A. Oda, H. Sugawara, and Y. Sakai, J. Phys. D **34**, 1919 (2001).
[22]M. A. Liberman and A. J. Lichtenberg, *Principles of Plasma Discharges and Materials Processing* (Wiley, New York, 1994), p. 318.
[23]K. Denpoh and K. Nanbu, Jpn. J. Appl. Phys., Part 1 **39**, 2804 (2000).
[24]R. N. Franklin, J. Phys. D **35**, 747 (2002).
[25]A. Picard, G. Turban, and B. Grolleau, J. Phys. D **19**, 991 (1986).
[26]J. L. Jauberteau, G. J. Meeusen, M. Haverlag, G. M. W. Kroesen, and F. J. Dehoog, J. Phys. D **24**, 261 (1991).
[27]D. H. Kim, C. M. Ryu, S. H. Lee, and J. K. Lee, Jpn. J. Appl. Phys. **47**, 7005 (2008).
[28]Z. Donkó and Z. Lj. Petrović, Jpn. J. Appl. Phys., Part 1 **45**, 8151 (2006).
[29]H. C. Kim and J. K. Lee, Phys. Plasmas **12**, 053501 (2005).
[30]V. M. Donnelly and M. J. Schabel, J. Appl. Phys. **91**, 6288 (2002).